Comparison of Deadzone and Vanderpol Oscillator Controlled Voltage Source Inverters in Islanded Microgrid

Vikash Gurugubelli, *Student Member, IEEE*
Department of Electrical Engineering
National Institute of Technology
Rourkela, India
vikas0225@gmail.com

Arnab Ghosh, *Senior Member, IEEE*
Department of Electrical Engineering
National Institute of Technology
Rourkela, India
aghosh.ee@gmail.com

Anup Kumar Panda, *Senior Member, IEEE*
Department of Electrical Engineering
National Institute of Technology
Rourkela, India
akpanda@nitrkl.ac.in

***Abstract*— This paper presents two types of nonlinear oscillator-based controllers termed virtual oscillator control (VOC). VOC is a time-domain control method unlike droop and virtual synchronous machine (VSM). In this method, each voltage source inverter (VSI) is tuned to mimic the dynamics of the nonlinearly coupled oscillators. Because VSIs are electrically coupled, they synchronize their output voltages and distribute the load in proportion to their ratings. Here, the authors presented two types of VOCs; one is nonlinear deadzone based VOC (NDZVOC) and the other is nonlinear vanderpol based VOC (NVPVOC). The design and implementation of the two control methods are presented in this work. The simulation study is conducted on the single-phase parallel VSIs system with the above-mentioned control methods during startup and load disturbance. Equal and unequal power-sharing is also presented in this study. The simulation results validate the proposed control methods.**

Keywords*— *Deadzone Oscillator, Vanderpol Oscillator, Voltage Source Inverter, Parallel operation, Microgrid

I. INTRODUCTION

Microgrids (MGs) have the potential to increase renewable energy (solar, wind, etc.) while also increasing reliability and lowering transmission line losses. This study is focusing on the parallel operation of inverters, which form an islanded MG. The main objectives of the islanded system are (i) Minimizing or reducing the communication between the inverters, which are operated in parallel. (ii) Despite load variations, ensuring system stability and synchronism between the inverters. (iii) Regulation of system frequency and (iv) proper power-sharing among the inverters. To achieve these objectives, we presented different control methods, which are inspired by the synchronization of coupled oscillators.

Droop control is a popular decentralized control method [1-2], in which the demerit is the high rate of change frequency (RoCF), the virtual synchronous machine concept introduced in [3-6], to mitigate the high RoCF problem. The VOC is a time-domain controller which reacts to the immediate current feedback signals without the need for additional filters or power calculations, which is a significant advantage in VOC [7, 8]. The VOC is a new advanced decentralised control technique for simulating the dynamic features of the limit cycle oscillators like the deadzone and vanderpol oscillator [9-11]. In [12], VOC was used in 1-phase MG, and in [13], it was implemented for a 3-phase MG. the need for a grid-tied inverter with VOC was stated in detail in [14]. An external loop was added in [15-16], to enable the VOC, to track the active and reactive power in grid-tied mode.

The contributions of this paper are (a) different VOC strategies applied to a system of 1-phase inverters, which are operated in parallel; (b) the design and implementation of the deadzone and vanderpol based VOC are presented clearly; (c) the simulation study is conducted with these two control methods during startup and load disturbance; (d) The equal and unequal power-sharing is also presented in this study; (e) finally, conclusions made-up on the two controllers based on the simulation results of the system.

This work is organized into six sections. The introduction is the first section; the second section includes the system description; the design and implementation of deadzone and vanderpol based VOC controllers are presented clearly in section 3. The 4, 5 sections are conditions for synchronization, and results and discussions, respectively. In section six, concluding remarks are made on the two control methods.

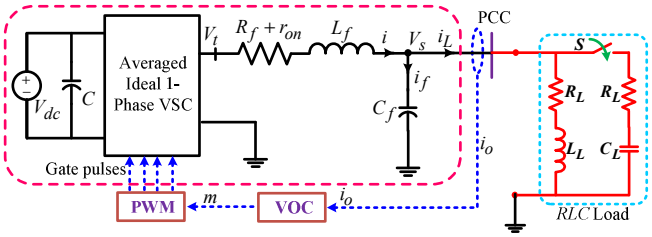

Fig. 1. Schematic diagram of a single-phase inverter with VOC

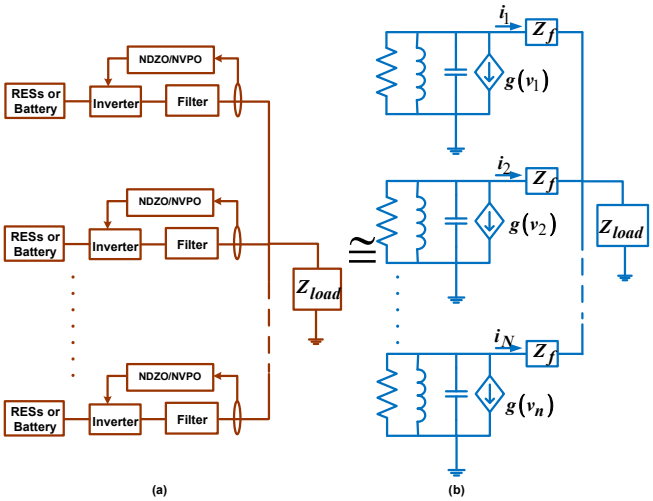

Fig. 2. The system of inverters in (a) will be controlled to emulate the system of coupled oscillators in (b).

II. SYSTEM DESCRIPTION

In this manuscript, the system is a simple single-phase VSI operating in standalone mode as shown in Fig. 1. The input dc supply is V_{dc}, which is time-varying and comes from RESs like PVs or fuel cells. The capacitor C is a DC-link capacitor, which regulates the dc bus voltage. R_f, L_f, and C_f are the filter resistance, inductance, and capacitor, respectively. r_{on} is the on-resistance of the IGBT switch. V_t is the terminal voltage of the inverter, which is before the filter. V_s is the inverter output voltage, which is after the

978-1-6654-4319-7/21/$31.00 ©2021 IEEE.

filter. I_f and I_L is the capacitor current and load current respectively. R_L, L_L, and C_L are the *RLC* load resistance, inductance, and capacitance, respectively. In this work, the inverter is controlled by using different oscillator-based controllers, such that it can give desired voltage and frequency. These oscillators are working on the current feedback signals. In this work, two different VO control techniques are presented, in which each inverter is operated to imitate the dynamics of either deadzone or vanderpol oscillator (detailed explanation of these oscillators presented in Section III). The dynamics of the MG system consisting of parallel single-phase VSIs is shown in Fig. 2(a) is regulated to mimic the system of coupled oscillators as shown in Fig. 2(b).

III. CONTROL STRUCTURES

A. *Nonlinear deadzone VOC (NDZVOC)*

This controller is inspired by the phenomenon of synchronization of non-linear oscillators in linear time-invariant systems. The schematic of the NDZVOC is shown in Fig. 3(a). This is having two subsystems, one is a parallel *RLC* circuit and the other subsystem $g(v_{C_1})$ is a voltage-dependent current source (VDCS), which is inspired by the DZ characteristics.

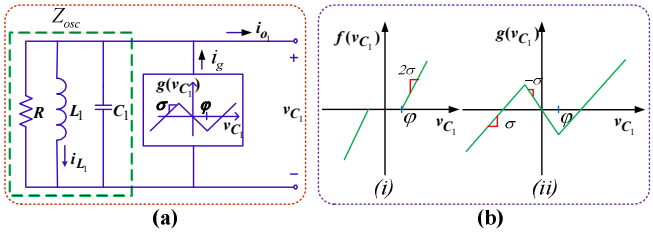

Fig. 3(a). Electrical schematic of the NDZVOC, 3(b). (*i*) DZ characteristics (*ii*) VDCS characteristics.

From Figs. 3b (*i* & *ii*), one can understand the characteristics of DZ and VDCS. Where $f(v_{C_1})$ is the DZ function as shown in (1)

$$f(v_{C_1}) = \begin{cases} 2\sigma(v_{C_1} - \varphi), v_{C_1} > \varphi \\ 0, \mid v_{C_1} \mid \leq \varphi \\ 2\sigma(v_{C_1} + \varphi), v_{C_1} < -\varphi \end{cases} \quad (1)$$

The dynamics of the oscillator inductor current, i_{L_1}, and the capacitor voltage, v_{C_1}, are given by [12-13].

$$\frac{dv_{C_1}}{dt} = \frac{1}{C_1}\left[(\sigma - \frac{1}{R})v_{C_1} - f(v_{C_1}) - i_{L_1} - i_{o_1}\right]$$
$$\frac{di_{L_1}}{dt} = \frac{v_{C_1}}{L} \quad (2)$$

The implementation of NDZVOC with single-phase inverters is shown in Fig. 4. The parameters of DZ oscillator-based VOC is shown in Table I.

Design and Parameter selection of NDZVOC:

In [7], the authors present the procedure for the design of NDZVOC parameters. The rated voltage is one of the design parameters k_{v_1}.

The following are the steps involved in the NDZVOC design approach

1. For desired output voltage of the inverter, set the parameter, i.e. voltage gain $k_{v_1} = \sqrt{2}V_{rated}$.
2. Under the no-load condition, the system attains maximum output voltage, according to tune the φ.
3. Under rated condition system operates at minimum voltage; tune the current gain k_{i_1} accordingly to get the minimum voltage at rated operation.
4. Select the values harmonic oscillator parameters L_1 and C_1, such that one can get the desired frequency i.e. $\omega = 1/\sqrt{LC}$.
5. The resistance, *R*, of the *RLC* subsystem and the slope of the deadzone function σ is selected to satisfy the Lienards theorem [12].
6. The remaining parameters of the NDZO is selected such that, the synchronization condition met, which is shown in equation (11).

Table I Parameters of DZO based VOC.

Description	Value
Voltage gain (k_{v_1})	$60\times\sqrt{2}$ (V/V)
Current gain (k_{i_1})	0.1125 (A/A)
Slope of DZO (σ)	1 (S)
Offset voltage (φ)	0.4695 (V)
DZO resistance (R)	10 (Ω)
DZO inductance (L_1)	500 (μH)
DZO capacitance (C_1)	14.1 (mF)

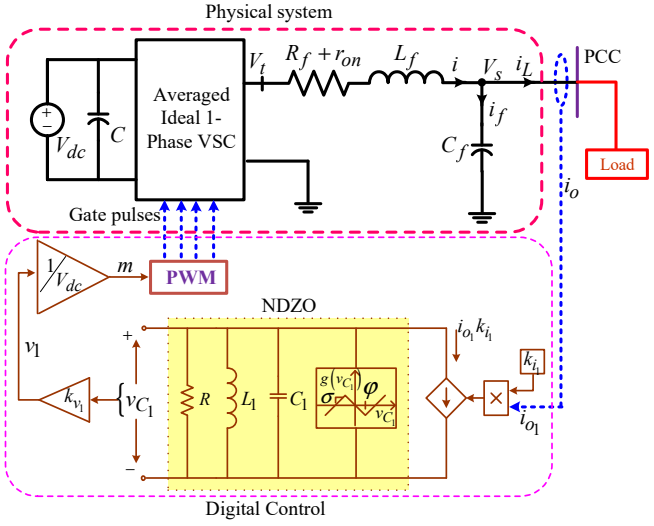

Fig. 4. Schematic of Implementation of NDZVOC with 1-phase VSI

B. *Nonlinear Vanderpol oscillator(NVPVOC)*

This controller is also inspired by the phenomenon of synchronization of non-linear oscillators in linear time-invariant systems. The schematic of the NVPVOC is shown in Fig. 5. The NVPVOC having two subsystems, one is a parallel *RLC* circuit and the other subsystem is a cubic nonlinear voltage-dependent current source [7].

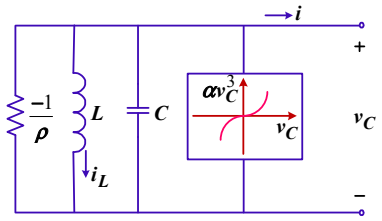

Fig. 5. An electrical schematic of the NVPVOC,

The dynamics of the oscillator inductor current, i_{L_2}, and the capacitor voltage, v_{C_2}, are given by

$$L_2 \frac{di_{L_2}}{dt} = \frac{v_2}{k_{v_2}}$$
$$C_2 \frac{dv_2}{dt} = -\alpha \frac{v_2^3}{k_{v_2}^2} + \rho v_2 - k_{v_2} i_{L_2} - k_{v_2} k_{i_2} i_{o_2} \quad (3)$$

The implementation of NVPVOC with single-phase inverters is shown in Fig. 6. The parameters of vanderpol oscillator-based VOC are shown in Table II.

Design and Parameter selection of NVPVOC:

The following equations from [7] are used to design the parameters of the NVPVOC. The scaling factors are shown in (4), the voltage regulation parameters are shown in (5), and the harmonic oscillator parameters are designed by using the equations (6-9).

$$k_{v_2} = V_{\max}, k_{i_2} = \frac{V_{\min}}{P_{\text{rated}}} \quad (4)$$

$$\alpha = \frac{2\rho}{3}, \rho = \frac{V_{\max}}{V_{\min}} \frac{V_{\max}^2}{V_{\max}^2 - V_{\min}^2} \quad (5)$$

$$\max\{C_{\min 1}, C_{\min 2}\} \le C_2 \le C_{\max} \quad (6)$$

$$C_{\min 1} = \frac{1}{2|\Delta\omega|_{\max}} \frac{V_{\max}}{V_{\min}} \frac{Q_{\text{rated}}}{P_{\text{rated}}} \quad (7)$$

$$C_{\min 2} = \frac{\rho}{8} \frac{1}{\omega^* \delta_{3:1}^{\max}} \quad (8)$$

$$C_{\max} = \frac{\rho}{6} t_{\text{rise}}^{\max} \quad (9)$$

Table II Parameters of VPO based VOC.

Description	Value
Voltage gain (k_{v_2})	63 (V/V)
Current gain (k_{i_2})	0.57 (A/A)
Conductance (ρ)	6.09 (Ω^{-1})
Coefficient of cubic current source (α)	4.06 (A/V^3)
VPO inductance (L_2)	3.99×10^{-5} (H)
VPO capacitance (C_2)	0.18 (F)

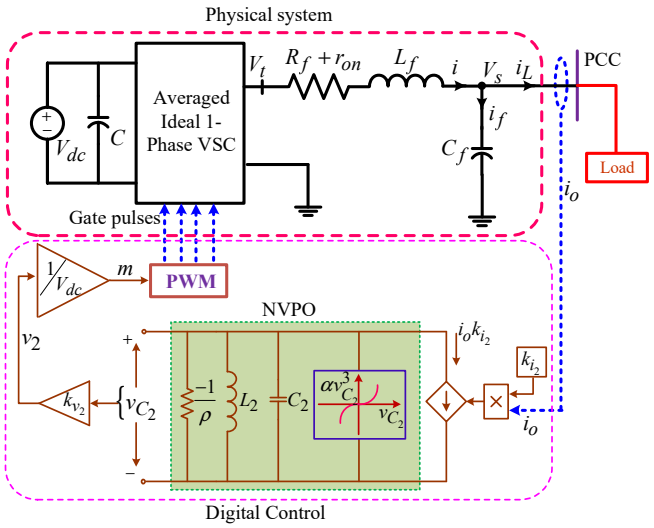

Fig. 6. Schematic of Implementation of NVPVOC with 1-phase VSI

IV. Conditions for Global Asymptotic Synchronization

The terminal voltages of the identical VSIs must be synchronized in a parallel operation system. The relationship between the physical VSI system and the VOC system is shown in Fig. 2, this translates to the VOC terminal voltage synchronizing. The global asymptotic synchronization condition of VOC terminal voltages was derived in [10] as shown in equation (10). The finding was extended in [12] to account for arbitrary current and voltage gains, yielding the following synchronization condition shown in equation (11)

$$\max_{\omega \in R} \left\| \frac{Z_f(j\omega) Z_{osc}(j\omega)}{Z_f(j\omega) + Z_{osc}(j\omega)} \right\| \sigma < 1 \quad (10)$$

$$\max_{\omega \in R} \left\| \frac{(k_{v_1} k_{i_1})^{-1} Z_f(j\omega) Z_{osc}(j\omega)}{(k_{v_1} k_{i_1})^{-1} Z_f(j\omega) + Z_{osc}(j\omega)} \right\| \sigma < 1 \quad (11)$$

Where Z_f and Z_{osc} are the equivalent filter impedance and impedance of the harmonic oscillator. From equations (10)-(11), synchronization criteria include several appealing characteristics. First, the synchronization conditions are unaffected by the load, number of VSIs, and their power ratings.

For stable operation of inverters and proper synchronization, the equivalent voltage fulfills the below equation shown in (12)

$$\frac{3\rho\beta}{2} V_{cr}^4 - \rho V_{cr}^2 - k_{v_2} k_{i_2} P_{cr} = 0 \quad (12)$$

After simplification [7],

$$V_{cr} = k_{v_2} \left(\frac{\rho + \sqrt{\rho^2 + 6 k_{v_2} k_{i_2} \rho\beta P_{cr}}}{3\rho\beta} \right)^{\frac{1}{2}}$$
$$= k_{v_2} \left(\frac{\rho + \sqrt{\rho^2 + 3\rho^2}}{9\alpha} \right)^{\frac{1}{2}} = k_{v_2} \sqrt{\frac{\rho}{3\alpha}} \quad (13)$$

Where $\beta = \frac{3\alpha}{k_{v_2}^2 \rho}$ and remaining parameters are mentioned in previous sections. The voltage of the inverters in NVPVOC should be higher than the critical voltage. As a result, the system is asymptotically stable locally.

V. Results and Discussions

Three 1-phase VSIs are connected in parallel in the simulation study. In which, each inverter uses an independent controller (either NDZO or NVPVOC). From tables I, II, and III, one can understand all the ratings and parameters of the system and controllers. The *RLC* load is shown in Fig. 1. In this simulation study, the authors considered two cases. The first case is equal power-sharing and the second case is unequal power-sharing.

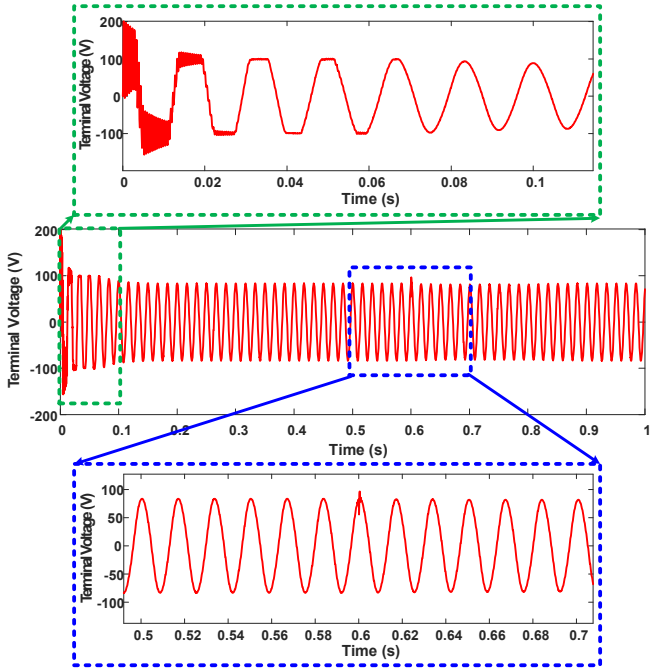

Fig. 7. Voltage synchronization waveforms during startup and load disturbance with 1: 1: 1 power-sharing (deadzone oscillator-based VOC).

Table III System parameters with the load and ac performance specifications.

Parameter	Value
PCC voltage	60 V (rms)
System frequency	60 Hz
R_f+$r_{on,}$ L_f & C_f	1 Ω, 6 mH & 1.2 µF
DC link voltage	100 V
R_L, L_L & C_L	50 Ω, 37 mH & 48 µF
Switching frequency	25 kHZ
$V_{\max}$ and $V_{\min}$	63 (V) and 57 (V)
P_{rated} and Q_{rated}	98.6 (W) and 17.12 (VAR)
$t_{\text{rise}}^{\max}$ and $\delta_{3:1}^{\max}$	0.2 (sec) and 2 (%)
ω^* and $\lvert\Delta\omega\rvert_{\max}$	2π 60 (rad/s) and 2π 0.5 (rad/s)

A. Case I(1:1:1 powersharing):

In this case, the power ratings of all the inverters are the same. The switch in Fig. 1 closed means the load is increasing. In a practical case, one cannot predict the initial conditions of the inverter. So, here the initial conditions of the inverters are 5V, 4 V, and 3V respectively. During startup and load disturbance, the voltage synchronization and current sharing of the inverters controlled with NDZVOC are shown in Fig. 7 and Fig. 8, respectively. The switch is initially at the open position, from 0.6 to 0.8 seconds, the switch at closed position (which means, the load step up and step down within 0.2 seconds). Similarly, the voltage synchronization and current sharing of the inverters controlled with NVPVOC are shown in Fig. 9 and Fig. 10, respectively.

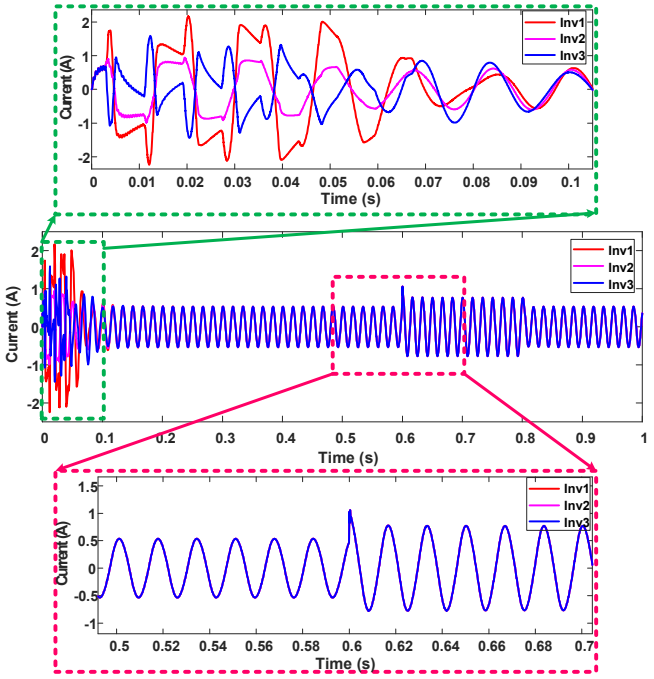

Fig. 8. Current sharing waveforms during startup and load disturbance with 1: 1: 1 power-sharing. (deadzone oscillator-based VOC).

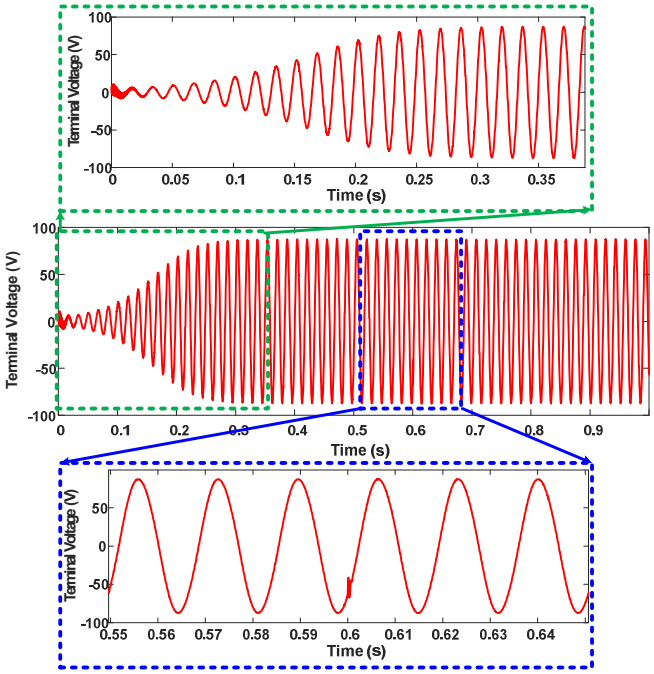

Fig. 9. Voltage synchronization waveforms during startup and load disturbance with 1: 1: 1 power-sharing (vanderpol oscillator-based VOC).

B. Case II(2:2:1 power-sharing):

In this case, the power ratings of all the inverters are unequal. In this case, also the initial conditions of the

inverters are 5V, 4 V, and 3V respectively. During startup and load disturbance, the voltage synchronization and current sharing of the inverters controlled with NDZVOC are shown in Fig. 11 and Fig. 12, respectively. The load disturbance is mentioned in the earlier section, same load disturbance is taken in this case also. Similarly, the voltage synchronization and current sharing of the inverters controlled with NVPVOC are shown in Fig. 13 and Fig. 14, respectively. In each figure, the authors zoomed the startup and load disturbance portions. During starting, the currents achieved a steady-state in 0.1 seconds in NDZVOC, whereas it takes more than 0.3 seconds in NVPVOC. As a result, NDZVOC has a better current sharing at startup than NVPVOC.

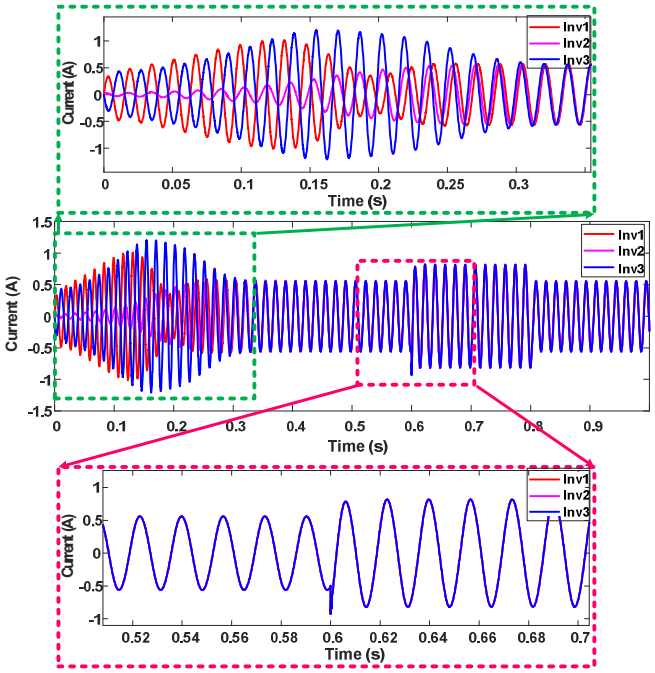

Fig. 10. Current sharing waveforms during startup and load disturbance with 1: 1: 1 power-sharing. (vanderpol oscillator-based VOC).

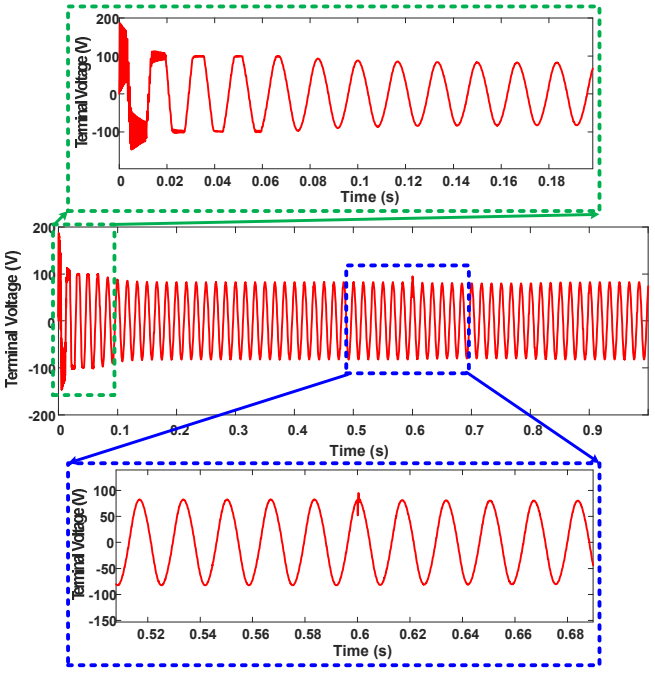

Fig. 11. Voltage synchronization waveforms during startup and load disturbance with 2: 2: 1 power-sharing (deadzone oscillator-based VOC).

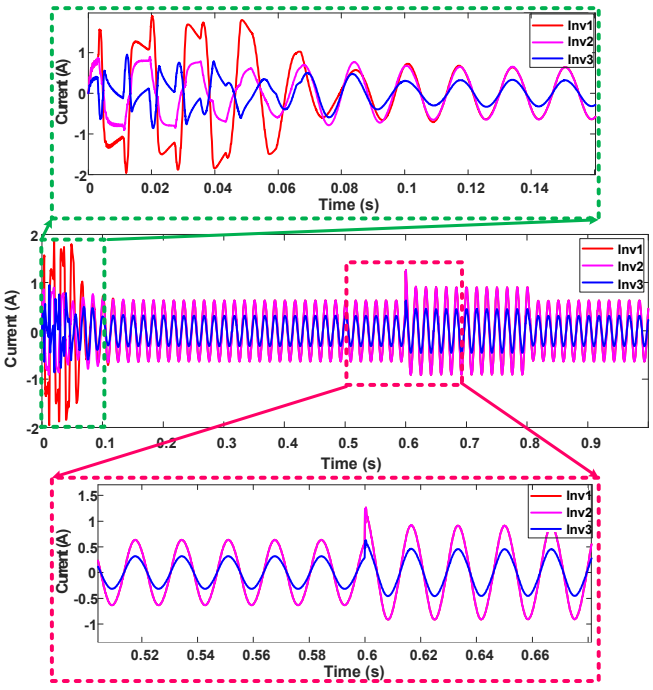

Fig. 12. Current sharing waveforms during startup and load disturbance with 2: 2: 1 power-sharing. (deadzone oscillator-based VOC).

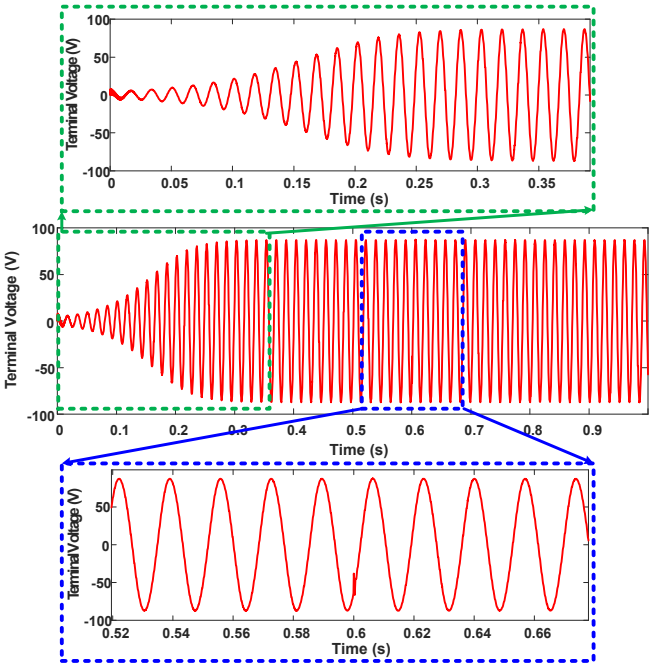

Fig. 13. Voltage synchronization waveforms during startup and load disturbance with 2: 2: 1 power-sharing (vanderpol oscillator-based VOC).

The voltage synchronization and current sharing are superior in both the controllers compared to conventional droop control methods. During startup, the voltage synchronization is very fast NDZVOC, but overshoot has existed. In, NVPVOC, the voltage synchronization is slow compared to NDZVOC, but there is no overshoot. During load disturbances, the current sharing and voltage synchronization are very prominent in both the control methods. The total harmonic distortion (THD) is also less in both the control methods as shown in Fig. 15. The voltage THD is a little less in NVPVOC compared to NDZVOC, but the current THD is less in NDZVOC compared to NVPVOC. In both the control methods, the third harmonic

is dominant, which is more than 1%. In NDZVOC, the THD is 1.97%, of which 1.95% is from the third harmonic component. In NVPVOC, the THD is 1.72%, which is 1.35% from the third harmonic component.

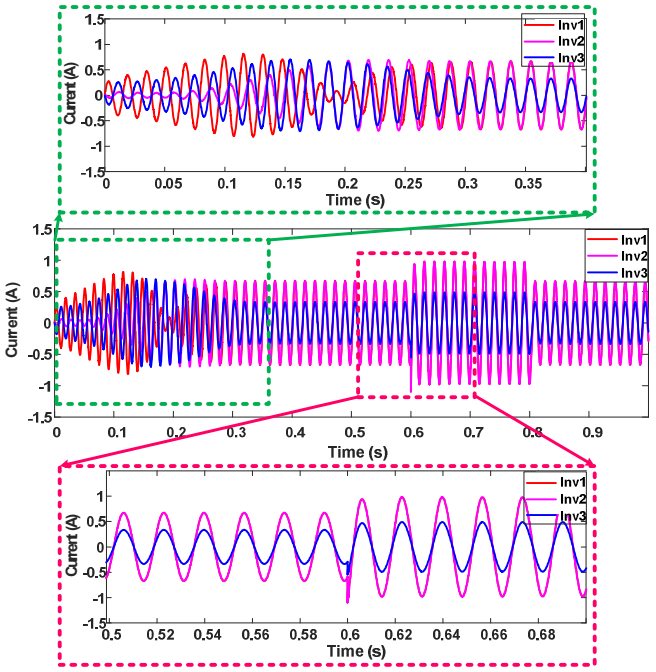

Fig. 14. Current sharing waveforms during startup and load disturbance with 2: 2: 1 power-sharing. (vanderpol oscillator-based VOC).

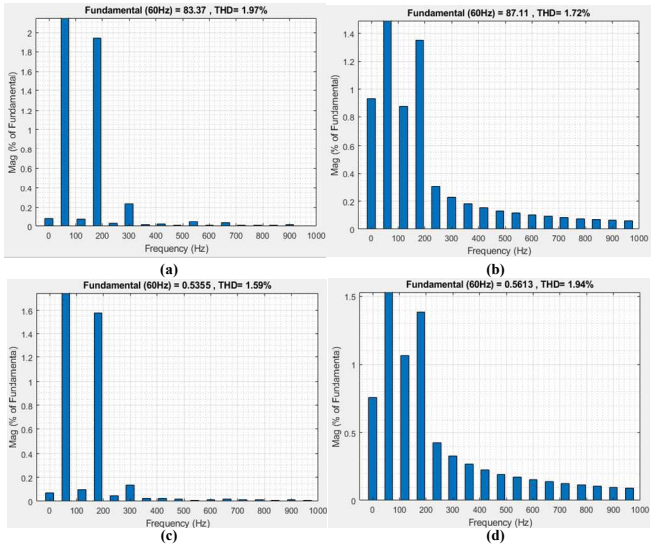

Fig. 15. THD in the voltage (a) NDZVOC (b) NVPVOC and THD in the current (c) NDZVOC (d) NVPVOC.

VI. Conclusion

Two different types of VOCs are applied to a parallel single-phase inverter system. Unlike droop and VSM, VOC is a time-domain control approach. In this, each VSI mimics the dynamics of nonlinear coupled oscillators. This work demonstrates the design and implementation of the above-mentioned control methods. During starting and load disturbance, the simulation study is conducted on a single-phase parallel VSIs system using the above-mentioned control approaches. This study also discusses equal and unequal power-sharing. During starting, NDZVOC has a better current sharing than NVPVOC. The voltage synchronization is very rapid in NDZVOC during starting, although there is an overshoot. The voltage synchronization in NVPVOC is slower than in NDZVOC, but there is no overshoot. Current sharing and voltage synchronization are prominent in both control approaches during load disturbances. The third harmonic is dominant in both control methods. The proposed control approaches are validated by the simulation results.

References

[1] J. C. Vasquez, J. M. Guerrero, M. Savaghebi, J. Eloy-Garcia, and R. Teodorescu, "Modeling, analysis, and design of stationary-reference-frame droop-controlled parallel three-phase voltage source inverters," *IEEE Transactions on industrial electronics*, vol. 60, no. 4, pp.1271-1280, Apr. 2012.

[2] G. Vikash, A. Ghosh, "Parallel Inverters Control in Standalone Microgrid using different Droop Control Methodologies and Virtual Oscillator Control," *Journal of The Institution of Engineers (India): Series B*, pp.1-9, Jun. 2021.

[3] A. Karimi, Y. Khayat, M. Naderi, T. Dragičević, R. Mirzaei, F. Blaabjerg, and H. Bevrani, "Inertia response improvement in AC microgrids: A fuzzy-based virtual synchronous generator control," *IEEE Transactions on Power Electronics*, vol. 35, no. 4, pp.4321-4331, Aug. 2019.

[4] G. Vikash, A. Ghosh, and S. Rudra, "Integration of Distributed Generation to Microgrid with Virtual Inertia," In *2020 IEEE 17th India Council International Conference (INDICON)*, Jul., 2020, pp. 1-6, IEEE.

[5] V. Gurugubelli, and A. Ghosh, "Control of inverters in standalone andgrid-connected microgrid using different control strategies," *World Journal of Engineering*, Jul. 2021.

[6] G. Vikash, D. Funde, and A. Ghosh, "Implementation of the Virtual Synchronous Machine in Grid-Connected and Stand-alone Mode," In *DC—DC Converters for Future Renewable Energy Systems, Springer, Singapore.,* 2022, pp. 335-353.

[7] B. B. Johnson, M. Sinha, N. G. Ainsworth, F. Dorfler, and S. V. Dhople, "Synthesizing virtual oscillators to control islanded inverters," *IEEE Trans. Power Electron.*, vol. 31, no. 8, pp. 6002–6015, Aug. 2016.

[8] V. Gurugubelli, A. Ghosh, A. K. Panda, and S. Rudra, "Implementation and comparison of droop control, virtual synchronous machine, and virtual oscillator control for parallel inverters in standalone microgrid," *International Transactions on Electrical Energy Systems,* vol. 31, no. 5, e12859, May. 2021.

[9] B. B. Johnson, S. V. Dhople, A. O. Hamadeh, and P. T. Krein, "Synchronization of nonlinear oscillators in an LTI electrical power network," *IEEE Trans. Circuits Syst. I: Reg. Papers*, vol. 61, no. 3, pp. 834–844, Mar. 2014.

[10] M. Sinha, F. Dörfler, B. B. Johnson, and S. V. Dhople, "Synchronization of Liénard-type oscillators in heterogenous electrical networks," in *Proc. Indian Control Conf.,* Jan., 2018, pp. 240–245.

[11] V. Gurugubelli, A. Ghosh, and A. K. Panda, "Different Oscillator Controlled Parallel Three-Phase Inverters in Standalone Microgrid," In *1st International Symposium on Sustainable Energy and Technological Advancements (ISSETA 2021)*, Sep. 2021.

[12] B. B. Johnson, S. V. Dhople, A. O. Hamadeh, and P. T. Krein, "Synchronization of parallel single-phase inverters with virtual oscillator control," *IEEE Trans. Power Electron.*, vol. 29, no. 11, pp. 6124–6138, Nov. 2014.

[13] B. B. Johnson, S. V. Dhople, J. L. Cale, A. O. Hamadeh, and P. T. Krein, "Oscillator-based inverter control for islanded three-phase microgrids," *IEEE J. Photov*, vol. 4, no. 1, pp. 387–395, Jan. 2014.

[14] M. Ali, H. I. Nurdin, and J. E. Fletcher, "Synthesizing averaged virtual oscillator dynamics to control inverters with an output LCL filter," *in Proc. 46th Annu. Conf. IEEE Ind. Electron. Soc.*, Oct., 2020, pp. 3265–3270.

[15] M. Ali, H. I. Nurdin, and J. Fletcher, "Dispatchable virtual oscillator control for single-phase islanded inverters: Analysis and experiments," *IEEE Trans. Ind. Electron.*, vol. 68, no. 6, pp. 4812–4826, Jun 2021.

[16] M. A. Awal, H.Yu, H. Tu, S. M. Lukic, and I. Husain, "Hierarchical control for virtual oscillator based grid-connected and islanded microgrids," *IEEETrans. Power Electron.*, vol. 35, no. 1, pp. 988–1001, Jan. 2020.